PROCEEDINGS OF
THE ROYAL SOCIETY A
MATHEMATICAL, PHYSICAL AND ENGINEERING SCIENCES

Nonlinear longitudinal stress coupling in glacier and ice sheet flow

Journal:	*Proceedings A*
Manuscript ID	RSPA-2025-0773
Article Type:	Research
Date Submitted by the Author:	05-Sep-2025
Complete List of Authors:	Mann, Logan; Dartmouth College, Thayer School of Engineering Warburton, Katarzyna; Dartmouth College, Department of Applied Mathematics and Theoretical Physics Meyer, Colin; Dartmouth College, Thayer School of Engineering
Subject:	Glaciology < EARTH SCIENCES, Applied mathematics < MATHEMATICS, Fluid mechanics < PHYSICS
Keywords:	glaciology, applied mathematics, fluid dynamics, longitudinal stress, green's function, nonlinear ice rheology, stress coupling, exact solution, ice streams, Shallow Shelf Approximation
Subject Category:	Earth Science

PROCEEDINGS A

royalsocietypublishing.org/journal/rspa

Research

Check for updates

Article submitted to journal

Subject Areas:
glaciology, applied mathematics, fluid dynamics

Keywords:
xxxx, xxxx, xxxx

Author for correspondence:
Logan E. Mann
e-mail:
logan.e.mann.th@dartmouth.edu

Nonlinear longitudinal stress coupling in glacier and ice sheet flow

L. E. Mann[1], K.L.P. Warburton[2] and C. R. Meyer[1]

[1]Thayer School of Engineering, Dartmouth College
[2]Department of Applied Mathematics and Theoretical Physics, University of Cambridge

The Greenland and Antarctic Ice sheets exhibit high variability in flow speed, over multiple orders of magnitude. Faster flow in ice streams, marine terminating glaciers, and ice shelves is described by the Shallow Shelf/Shelfy-Stream Approximation (SSA), which requires a nonlocal balance between driving stress, friction at the ice-bed interface, and longitudinal/membrane stresses. Nonlocal stresses mediate spatial variability in ice flow, over a finite length scale, known as the longitudinal coupling length, which determines how far viscous stresses may be transmitted in glaciers and ice sheets. The strongly nonlinear rheology of ice complicates the stress transmission, but previous work has relied on either linear-Newtonian models or linearized, small-perturbation models, to determine the coupling length. Here, we derive new exact solutions to SSA, which explain how nonlinear feedbacks between the stress state and the nonlinear rheology of ice determine the coupling length. For complex and multi-scale flow fields, these exact solutions provide a foundation for approximations that can reconstruct the effects of a nonlocal stress balance, given input data for the driving stress and friction fields.

THE ROYAL SOCIETY PUBLISHING

1. Introduction

The Greenland and Antarctic ice sheets evolve as incompressible, viscous, slow, and shallow non-Newtonian fluids over seasonal to millennial timescales. They are shallow in that all reasonable vertical and horizontal scales lead to small aspect ratios, asymptotically reducing the ice sheet dynamics to thin-film approximations with rigorous small-parameter arguments [1]. However, the large range of ice flow velocities observed in ice sheets imposes a dichotomy between two end-member thin film flow regimes. At the largest scales, ice sheet dynamics are well-described by the classical lubrication approximation, called the Shallow Ice Approximation in the glaciology literature (hereafter denoted as SIA; [2–6]). SIA imposes a canonical no-slip boundary condition at the ice base, meaning hydrostatic pressure gradient forces (called driving stress in the glaciology literature and hereafter) are entirely accommodated by vertical shear deformation. In the SIA model, ice velocity is strictly a function of local driving stress, computed from the no-slip, infinite in extent slab-on-a-slope solution to the Stokes dynamics. By contrast, fast flowing regions of grounded ice (order 100 m yr^{-1} or faster), called ice streams, and free floating regions of ice, called ice shelves, are better described by free film models [7], called the Shallow Shelf/Shelfy-Stream Approximation in the glaciology literature (hereafter denoted as SSA; [4,8,9]). In the SSA model, traction at the bed is considered negligible, so driving stress is primarily balanced by slip at the ice base and membrane stresses rather than vertical shear stress. Membrane stress is a general term which describes both longitudinal deviatoric stresses in the normal horizontal direction, i.e. τ_{xx} or τ_{yy}, and lateral shear deviatoric stresses that are transverse to flow, i.e. τ_{xy}. SSA reduces this ice sheet stress balance to a nonlinear elliptic momentum equation, where driving stress acts as an inhomogenous forcing term. Therefore, in fast flow regimes, ice flow at any one location is not strictly a function of the local driving stress. Instead, membrane stresses mediate the transmission of stresses between different locations.

Longitudinal/membrane stresses are apparent in boundary layers, which emerge in the flow field in response to sharp transitions in driving stress or friction. For example, if friction decreases in the downstream region of an ice stream, the upstream region will experience a pulling force from this faster downstream ice, causing it to also accelerate despite no change in the local friction. However, the downstream ice will also experience a pulling force from the upstream ice, preventing it from accelerating as much as it would if the velocity only depended on the local driving stress and friction. An extensional longitudinal stress results in a smooth spatial transition, in a finite boundary layer, from slower upstream ice to faster downstream ice. The opposite change, an increase in friction for downstream ice, would result in compressive longitudinal stress. Longitudinal stress could also be induced by a change in driving stress.

In these boundary layers, perturbations to the stress state result in changes to ice flow over a finite length scale, the longitudinal coupling length (LCL) [10–12]. In this sense, the longitudinal coupling length can be thought of as the transmissivity of stress in glaciers and ice sheet, smoothing variability on length scales less than the LCL. Changes in driving stress or basal friction over spatial scales much greater that the LCL allow longitudinal stress coupling to be ignored. However, the literature often relies on order of magnitude estimates of the LCL to explain observed phenomena [10]. In real glaciers and ice sheets, flowing over realistic bed topographies and complex subglacial hydrologic systems, pressure and friction gradients can occur over multiple scales, and it is not always clear whether flow is dominated by local driving stress or longitudinal stress gradients from surface velocity observations, particularly for fast flowing grounded ice. Identifying more precise formulations of the LCL, taking into account short-scale effects, is important to distinguish these two modes, unraveling the processes behind emergent phenomena.

Observations of glacier velocities that deviated from local stress calculations prompted a consideration of longitudinal stress gradients [13]. Early work developed an approximate theoretical approach, based on running local averaging windows of arbitrary length [14–16]. Kamb and Echelmeyer (1986; [10,17–19]) improved on these approaches. They considered

longitudinal stresses as a kind of low-pass filter, which smoothed short-wavelength surface and basal perturbations in the flow field. They derived Green's function solutions and LCL scalings from a vertically integrated and linearized model, to superimpose the effect of perturbations to the flow field. This approach is effective when stress perturbations remain small enough for linearization about the mean stress field, but it applies a fundamentally linear conception of superposition to governing equations that are by nature nonlinear.

Other approaches have aimed to diagnose the LCL empirically, taking advantage of the increased resolution and availability of surface velocity observations. O'Neel and Pfeffer (2005; [20]) imposed a top-down force balance analysis on surface velocity measurements from 1977-2001, to capture the retreat of Columbia Glacier, Alaska, demonstrating that ice velocity showed little correspondence to driving stress during the retreat. Kavenaugh and Cuffey (2009; [21]) inverted for the longitudinal coupling length by relating thickness to a smoothing window which provided the best match to surface velocity observations. Their results displayed the limitation of Kamb and Echelmeyer's approach, when applied to large and multi-scale longitudinal variations. Enderlin et al. (2016; [11]) considered flow dominated by basal slip, inverting for the longitudinal coupling length from high resolution surface velocity measurements, determining correlations between the relevant environmental parameters and the derived longitudinal coupling lengths.

More recent theoretical approaches to longitudinal stress problems still rely on linearly viscous models [12,22–29] or asymptotic linearizations about a background stress state [30–33], or some combination of both. Barcilon and Macayeal (1993; [22]) derived an exact solution to the linear stokes equations for an extreme case, transition between no-slip and free-slip at the bed. They captured many of the essential features of these boundary layer systems and provided a useful benchmark for numerical experiments. Gudmundson (2003; [31]) evaluated the time-dynamic transmission of basal variability to the glacier surface, also with a linearly viscous Stokes flow, thinking of the longitudinal stress problem as a problem of information transfer. Hindmarsh (2004; [32]) applied a similar method, linearizing the nonlinear Stokes equations to evaluate the performance of the various approximations used in numerical ice sheet modeling, demonstrating that the qualitative forms of Gundmundsson's solutions also occurred with nonlinear rheologies. Mantelli et al. (2019a, [25]) returned to the the sudden onset of slip, studied by Barcillon and MacAyeal, exploring inconsistencies that arise when coupling viscous ice flow models to a thermal model, which had previously been identified by Fowler (2001; [34]). Rines et al. (2024; [12]) developed a vertically averaged linear Newtonian model, capable of smooth transitions between vertical shear dominated and slip dominated flow. This well-describes some essential relationships between the thickness, slope, and friction to the longitudinal coupling length.

However, the nonlinear rheology of ice complicates nonlocal stress coupling. Ice rheology is typically modeled empirically with a power law shear thinning rheology [35]. Flow velocity therefore obeys nonlinear governing equations, coupling ice rheology and stress transmission. This complicates analysis of stress coupling in glaciers and ice sheets, which still largely relies on linearized descriptions to derive the LCL.

In this study, we derive the relevant scales and parameters which determine the nonlinear mechanics of longitudinal stress boundary layers in fast flowing ice streams, characterized by relatively low driving stress and fast flow velocity over weak beds. In Section 2, we explain the governing equations and consider some identities arising from a weighted averaging ansatz. Next, we rely on these identities to interpret the LCL from a scaling analysis. In Section 3(a), we derive novel exact solutions to SSA for isothermal ice streams of constant thickness with either sudden changes in driving stress or sudden changes in friction at the bed. We then show that we can use our exact solutions to distinguish between longitudinal stress and strain-rate LCLs. In Section 3(b) we use the exact solutions to reconstruct approximate solutions for continuous friction or driving stress, pointing out the applicability to less idealized scenarios. In the discussion and conclusions sections 4-5, we discuss general principles of nonlinear stress coupling and potential applications of this work.

royalsocietypublishing.org/journal/rspa Proc R Soc A 0000000

2. Methods

(a) Governing equations

We consider the flow of an incompressible, viscous, and laterally unconfined ice sheet. Because the ice sheet is unconfined, flow is laterally uniform, reducing the problem to the 2D flow field, $\mathbf{u} = (u, v)$, in coordinates, (x, z), where x is oriented in the along flow direction and z is aligned with gravity. The viscous flow of ice is described by shear-thinning rheology, described empirically by the power law expression

$$\tau_{ij} = A^{-1/n} \dot{\varepsilon}^{\frac{1-n}{n}} \dot{\varepsilon}_{ij} \tag{2.1}$$

where the deviatoric stress tensor, $\tau_{ij} = \sigma_{ij} + \delta_{ij} p$, is defined as the non-hydrostatic component of the Cauchy stress tensor, σ_{ij}, given here in terms of the pressure field, p, and $\dot{\varepsilon}_{ij} = \frac{1}{2}\left(\partial_i u_j + \partial_j u_i\right)$ is the strain-rate tensor. In glaciology the rheology of ice is typically defined by two empirical parameters, the coefficient, A, and the exponent, n, (usually taken between 3 and 4. Here we take $n = 4$ [36]). $\dot{\varepsilon}$ is the effective strain-rate, given by the second tensor invariant, $\dot{\varepsilon}^2 = \frac{1}{2}\sum_{ij} \dot{\varepsilon}_{ij}\dot{\varepsilon}_{ij}$.

For shallow, fast flowing ice streams, vertical deformation is negligible to the stress balance, allowing depth integration of the stokes equations to the Shallow Shelf/Stream Approximation (SSA) [1,9].

$$2\frac{d}{dx}\left(HA^{-1/n}\left|\frac{du}{dx}\right|^{\frac{1-n}{n}}\frac{du}{dx}\right) - C\,|u|^{m-1}\,u = -\tau_d \tag{2.2}$$

which is a 2nd-order, inhomogenous, nonlinear differential equation for the velocity field, u, . The driving stress $\tau_d = -\rho g H \frac{ds}{dx}$ acts as an inhomogenous forcing, where ρ is the density of ice, g is gravitational acceleration, and $\frac{ds}{dx}$ is the surface slope. This forcing is balanced by resistive stresses at the bed controlled by the friction coefficient, C, and longitudinal stress gradients, which mediate longitudinal variations in friction or driving stress.

The simplest possible solution to this model emerges given a parallel slab, with a constant thickness H, on a constant slope, $\frac{ds}{dx}$, with a constant friction coefficient, C, (figure 1a). For this 'slab-on-a-slope' model, longitudinal stresses vanish, and the solution is given by

$$U = \frac{|\tau_d|^{\frac{1}{m}-1}\,\tau_d}{C^{\frac{1}{m}}}. \tag{2.3}$$

We hereafter call this solution, U, the 'local solution', because the absence of longitudinal stress means that ice flow velocity is only a function of the local driving stress, τ_d, and local friction at the bed C.

(b) Weighting function solutions

If we consider a step-change in either slope or friction at $x = 0$, following the schematic in figure 1a-b, a discontinuity arises in the local solution as velocity suddenly jumps from velocity U_A to velocity U_B across this boundary,

$$U(x) = U_A + (U_B - U_A)\Theta(x) = \begin{cases} U_A & \text{if } x < 0 \\ U_B & \text{if } x \geq 0 \end{cases} \tag{2.4}$$

where $\Theta(x)$ is the Heaviside step function. This would violate both momentum and mass continuity, and du/dx, neglected above, becomes infinite. Therefore, if any change in friction or driving stress occurs, longitudinal stresses must play a role in mediating that contradiction across a boundary layer, through a smooth velocity field.

In this paper, we derive exact solutions to such step-change problems, including longitudinal stress, but we begin with an intuitive approach. If we consider the driving stress field, $\tau_d(x)$, as a forcing to an inhomogenous 2nd-order ODE (as 2.2 implies), it should be possible to solve for the ice velocity, $u(x)$, given the driving stress field as input data, modulated by the friction field, $C(x)$. This informs our ansatz: if the flow of ice in any one location depends on both local stresses

royalsocietypublishing.org/journal/rspa Proc R Soc A 0000000

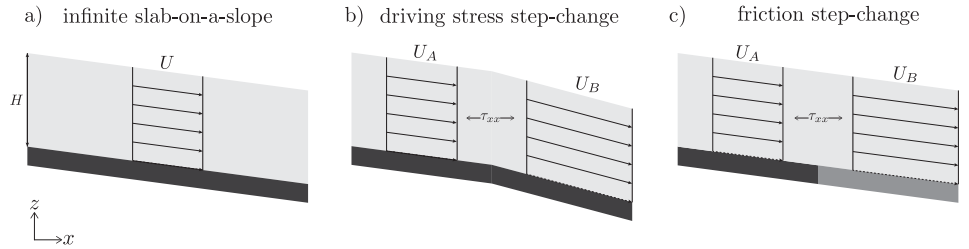

Figure 1. a) The constant thickness, infinite slab-on-a-slope: This is the simplest possible exact solution to SSA, being the only scenario where longitudinal stress gradients are absent. b) The driving stress step change: A longitudinal stress gradient is induced by a sudden change in both surface and bed slope, maintaining a constant thickness. c) The friction step-change: A longitudinal stress gradient is induced by a sudden change in friction at the bed, maintaining a constant thickness.

and on far field stresses, then the velocity field $u(x)$ must be a continuous weighted average of the local solution at every point.

$$u(x) = \int_{-\infty}^{+\infty} w(x-\xi)U(\xi)d\xi, \tag{2.5}$$

where $w(x)$ represents a weighting function which modifies the integral kernel. Therefore, if one can determine the correct weighting function, $w(x)$, the local velocity $U(x)$ can be used as input data to determine $u(x)$. For linearly viscous fluids, where $n=1$, $w(x)$ is the Green's function for (2.2), i.e. a solution for $w(x)$ could be applied to arbitrary forcings, $U(x)$. However, Green's functions do not normally exist for nonlinear differential equations. We expand on this distinction in section 3(b).

From (2.5), we can derive an identity which relates the weighting function $w(x)$ to the longitudinal strain-rate, $\frac{du}{dx}$, by differentiating inside the integral, applying the chain rule, and integrating by parts, assuming that $w(x)$ must decay to 0, as longitudinal stresses vanish in the far field, we obtain

$$\begin{aligned} \frac{du}{dx} &= \int_{-\infty}^{+\infty} w(x-\xi)\frac{dU}{d\xi}d\xi \\ &= (U_B - U_A)\int_{-\infty}^{+\infty} w(x-\xi)\delta(\xi)d\xi \end{aligned} \tag{2.6}$$

where $\delta(x)$ is the Dirac delta function. The integral definition of δ leads us to an identity, which relates the weighting function to longitudinal strain-rates in our problem.

$$\frac{du}{dx} = (U_B - U_A)w(x) \tag{2.7}$$

This identity expresses that for step-change problems, the weighting function $w(x)$ is a straightforward function of the strain-rate, $\frac{du}{dx}$, and the step-change, $U_B - U_A$.

This allows us to extract $w(x)$ from numerical ice sheet simulations. In figure 2, we solve (2.2) numerically, with the finite element package Firedrake [37], and calculate $w(x)$ through finite differences of the velocity field, $u(x)$. One could also apply this scheme to any other ice sheet model (in place of (2.2)) and extract the corresponding weighting function. This reveals the essential structure of longitudinal stress boundary layers. The effect on the flow field decays away from the location of the perturbation ($x=0$). In the next section, we will explore this identity as a variable transform allowing for exact solutions to the step-change problem in SSA.

royalsocietypublishing.org/journal/rspa Proc R Soc A 0000000

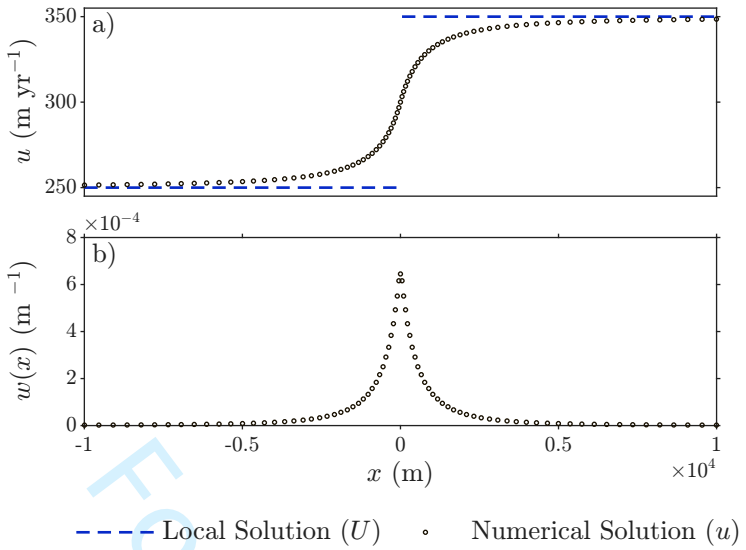

Figure 2. a) Circle markers indicate the numerical solution to (2.2), using the finite element package firedrake, for a change in driving stress from velocity $a = 250$ m yr^{-1}, to velocity $b = 350$ m yr^{-1}. Blue dotted line shows the local solution, U, which is the (discontinuous) solution to SSA with longitudinal stress gradients neglected. b) Shows the weighting function, computed from the numerical solution, which is greatest in the center of the boundary layer and decays towards 0 in the far field.

(c) Deriving the longitudinal coupling length

We posit that the weighting function $w(x)$ must decay according to a characteristic length scale, ℓ, which can be determined through scaling of the governing equations. Differentiating (2.2) gives

$$2\frac{d^2}{dx^2}\left(HA^{-1/n}\left|\frac{du}{dx}\right|^{\frac{1-n}{n}}\frac{du}{dx}\right) - \frac{dC}{dx}|u|^{m-1}u - Cm|u|^{m-1}\frac{du}{dx} = -\frac{d\tau_d}{dx}. \tag{2.8}$$

Inserting our weighting function identity, $\frac{du}{dx} = (U_B - U_A)w$, we obtain

$$2|U_B - U_A|^{\frac{1-n}{n}}(U_B - U_A)\frac{d^2}{dx^2}\left(HA^{-1/n}|w|^{\frac{1-n}{n}}w\right) - \frac{dC}{dx}|u|^{m-1}u - Cm|u|^{m-1}(U_B - U_A)w = -\frac{d\tau_d}{dx} \tag{2.9}$$

and nondimensionalize the problem according to the scales

$$\begin{aligned} x &= \ell\hat{x}, & w &= \frac{1}{\ell}\hat{w}, & \delta &= \frac{1}{\ell}\hat{\delta}, & H &= [H]\hat{H}, \\ A &= [A]\hat{A}, & C &= [C]\hat{C}, & \tau_d &= [\tau_d]\hat{\tau}_d, & u &= [U]\hat{u} \end{aligned} \tag{2.10}$$

where ℓ is the longitudinal coupling length scale, and [ ] brackets denote characteristic values of the respective variables. Further, we nondimensionalize the local velocity as $U = [U]\hat{U}$, where we define the velocity scale as the average local velocity, $[U] = \bar{U} = \frac{U_A + U_B}{2}$ and thus establish a relationship between the velocity, driving stress, and friction scales informed by (2.3).

$$[U]^m = \frac{[\tau_d]}{[C]}. \tag{2.11}$$

By defining ℓ as

$$\ell = \left(\frac{2[H]}{[C][A]^{1/n}}\frac{|U_B - U_A|^{\frac{1-n}{n}}}{[U]^{m-1}}\right)^{\frac{n}{n+1}}, \tag{2.12}$$

(2.13) simplifies to

$$\frac{d^2}{d\hat{x}^2}\left(\hat{H}\hat{A}^{-1/n}|\hat{w}|^{\frac{1-n}{n}}\hat{w}\right) - m\hat{C}|\hat{u}|^{m-1}\hat{w} = \frac{[U]}{U_B - U_A}\left(\frac{d\hat{C}}{d\hat{x}}|\hat{u}|^{m-1}\hat{u} - \frac{d\hat{\tau}_d}{d\hat{x}}\right). \tag{2.13}$$

Thus the weighting function is controlled by ℓ and the nondimensional coefficients: n, which controls the nonlinearity of the ice rheology, m, which determines the nonlinearity of the sliding law, and $[U]/(U_B - U_A)$ which describes the ratio of the velocity scale to the step-change in the local velocity.

3. Results

(a) Exact solutions

In this work, we identify exact solutions to two special cases of (2.13) involving: (1) A step-change in driving stress (figure 1a) and (2) a step-change friction (figure 1b). If we assume a constant ice thickness H, constant rheology coefficient, A (corresponding to a constant temperature), and linear sliding, $m = 1$, then (2.13) simplifies to (dropping the $\hat{}$ symbol for convenience)

$$\frac{d^2}{dx^2}\left(|w|^{\frac{1-n}{n}}w\right) - Cw = \frac{[U]}{U_B - U_A}\left(\frac{dC}{dx}u - \frac{d\tau_d}{dx}\right). \tag{3.1}$$

In the driving stress case, we consider a sudden change in both surface and bed slope (and thus driving stress), but friction remains constant, reducing (3.1) to

$$\frac{d^2}{dx^2}\left(|w|^{\frac{n-1}{n}}w\right) - w = -\delta(x). \tag{3.2}$$

In the friction case, we consider a sudden change in friction coefficient, while driving stress is held constant (i.e. parallel slab), reducing (3.1) to

$$\frac{d^2}{dx^2}\left(|w|^{\frac{1-n}{n}}w\right) - U(x)^{-1}w = -U(x)^{-2}u\delta(x). \tag{3.3}$$

Both problems are subject the the boundary conditions,

$$w \to 0, \text{ as } |x| \to \infty \tag{3.4}$$

such that the longitudinal strain-rate approaches 0 in the far-field.

In this section, we present exact solutions for both of the above problems, for both linear Newtonian $(n = 1)$ and nonlinear strain-weakening $(n > 1)$ viscous fluids.

(i) Driving stress step-change

First, we consider the driving stress step-change problem. We integrate the second order ODE in (3.2) on the interval $-\epsilon < x < +\epsilon$, where ϵ is a small parameter, to derive a matching condition at the driving stress discontinuity

$$\begin{gathered}\int_{-\epsilon}^{+\epsilon}\left\{\frac{d^2}{dx^2}\left(|w|^{\frac{1-n}{n}}w\right) - w\right\}dx = -\int_{-\epsilon}^{+\epsilon}\delta(x), \\ \frac{d}{dx}\left(|w|^{\frac{1-n}{n}}w\right)\Big|_{-\epsilon}^{+\epsilon} - 0 = -1.\end{gathered} \tag{3.5}$$

Then, we derive general solutions to (3.2) on to intervals $x \in [-\infty, -\epsilon]$ and $x \in [+\epsilon, +\infty]$ and we use both the boundary conditions (3.4) and the matching condition (3.5) to determine exact

royalsocietypublishing.org/journal/rspa Proc R Soc A 0000000

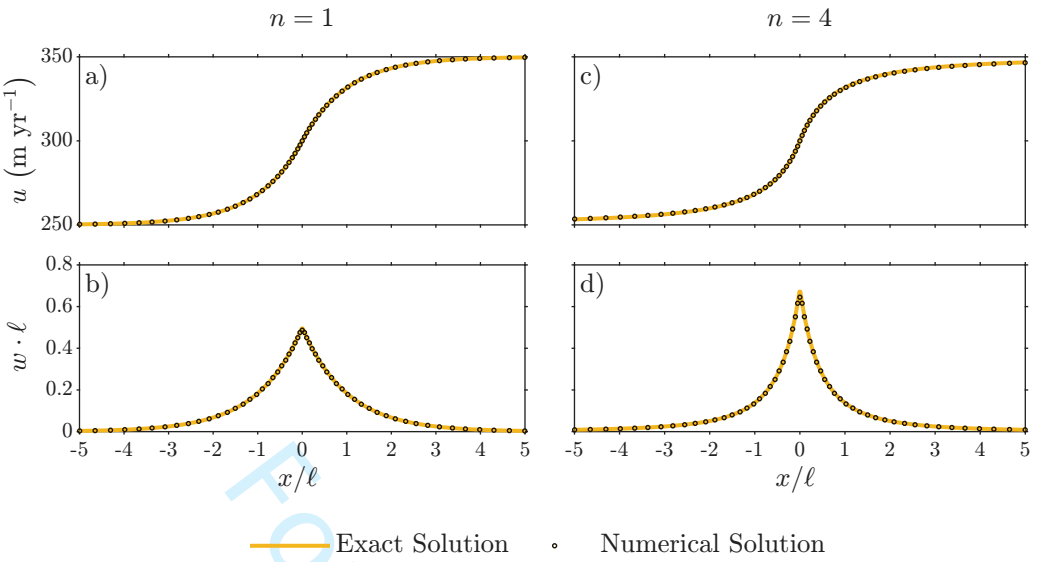

Figure 3. Exact (solid line) and numerical (○ markers) solutions to SSA (2.2), subject to a driving stress step-change, for both linear-Newtonian ($n = 1$; left column) and nonlinear shear-thinning ($n = 4$; right column) ice: a,c) Velocity field, u. b,d) Weighting function, w, nondimensionalized about $1/\ell$.

solutions for the entire domain

$$w(x) = \begin{cases} \frac{1}{2}e^{-|x|}, & n = 1 \\ \left(\frac{n-1}{2}\sqrt{\frac{2}{n+1}}|x| + \left(\frac{1}{2}\sqrt{\frac{n+1}{2}}\right)^{-\frac{n-1}{n+1}} \right)^{-\frac{2n}{n-1}}, & n \neq 1 \end{cases}. \tag{3.6}$$

We note that the mathematical structure changes between $n = 1$ and $n \neq 1$ upon integration, because the nonlinear integration requires that $n \neq 1$.

For the driving stress step-change problem, we arrive at an exact solution to the velocity field, $u(x)$, by integrating the identity $\frac{du}{dx} = \frac{(U_B - U_A)}{\bar{U}} w(x)$ on both intervals, applying the fundamental theorem of calculus

$$\int_{-\infty}^{x} \frac{du}{d\xi} d\xi = \frac{U_B - U_A}{\bar{U}} \int_{-\infty}^{x} w(\xi) d\xi, \quad x \in [-\infty, -\epsilon] \tag{3.7a}$$

$$\int_{x}^{+\infty} \frac{du}{d\xi} d\xi = \frac{U_B - U_A}{\bar{U}} \int_{x}^{+\infty} w(\xi) d\xi, \quad x \in [\epsilon, \infty] \tag{3.7b}$$

$$u(x) = \begin{cases} U(x) - \operatorname{sgn}(x) \frac{U_B - U_A}{\bar{U}} \frac{1}{2} e^{-|x|}, & n = 1 \\ U(x) - \frac{U_B - U_A}{\bar{U}} \operatorname{sgn}(x) \sqrt{\frac{2}{n+1}} \left(\frac{n-1}{2}\sqrt{\frac{2}{n+1}}|x| + \left(\frac{1}{2}\sqrt{\frac{n+1}{2}}\right)^{-\frac{n-1}{n+1}} \right)^{-\frac{n+1}{n-1}}, & n \neq 1 \end{cases} \tag{3.8}$$

The exact solutions (3.6) and (3.8) are depicted in figure 3.

As expected, the weighting function decays from the center of the boundary layer to 0 in the far field. If $n = 1$, this is a straightforwardly exponential decay, but if $n > 1$, this decay is different in character, with a higher peak w and a shorter decay length, because ℓ is inversely proportional to the absolute value of the step change, $\ell \sim |U_B - U_A|^{-\frac{n-1}{n+1}}$, for $n > 1$, but this dependence vanishes in the linear case when $n = 1$.

(ii) Sliding step-change

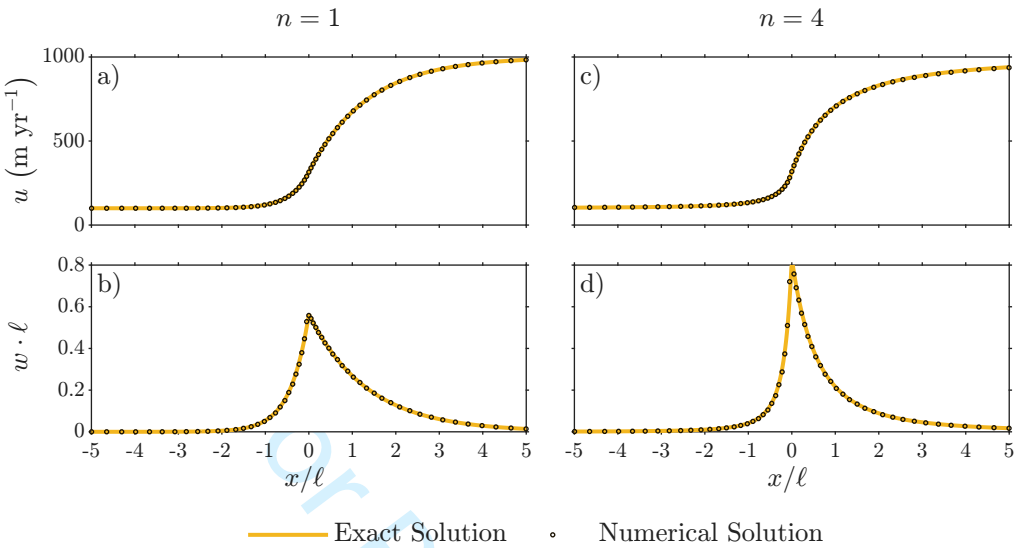

Figure 4. Exact (solid line) and numerical (cicle markers) solutions to SSA (2.2), subject to a step-change in friction, for both linear-Newtonian ($n = 1$; left column) and nonlinear shear-thinning ($n = 4$; right column) ice. a,c) Velocity field, u. b,d) Weighting function, w, nondimensionalized about $1/\ell$.

Next, we consider a step-change in friction coefficient. We can perform a similar procedure as in Section 3a(i) to arrive at general solutions to (3.3) on $x \in [-\infty, -\epsilon]$ and $x \in [\epsilon, \infty]$. We apply the boundary condition (3.4) and an assumption of continuity to reduce the general solutions to

$$w(x) = \begin{cases} C_2 e^{\frac{x}{\sqrt{U_A/\bar{U}}}}, & x \in [-\infty, -\epsilon] \\ C_2 e^{-\frac{x}{\sqrt{U_B/\bar{U}}}}, & x \in [\epsilon, +\infty] \end{cases} \tag{3.9}$$

for the Newtonian case ($n = 1$) and

$$w = \begin{cases} \left(-\frac{n-1}{2}\sqrt{\frac{2}{n+1}}\frac{x}{\sqrt{U_A/\bar{U}}} + C_2 \right)^{-\frac{2n}{n-1}}, & -\infty < x < -\epsilon \\ \left(\frac{n-1}{2}\sqrt{\frac{2}{n+1}}\frac{x}{\sqrt{U_B/\bar{U}}} + C_2 \right)^{-\frac{2n}{n-1}}, & +\epsilon < x < +\infty \end{cases} \tag{3.10}$$

the non-Newtonian case ($n \neq 1$). The appearance of C_2 on both sides of the interval is a consequence of $w(x)$ being continuous at $x = 0$.

While similar in character to the driving stress step-change problem, subtle properties of the delta function [38] require a different approach to solution, primarily in the derivation of matching conditions at $x = 0$. We can solve for the undetermined coefficients of general solutions (3.9-3.10), by integrating the identity $\frac{du}{dx} = (U_B - U_A)w(x)$ on both intervals and matching. This leads to exact solutions for the weighting function on the entire domain

$$w(x) = \begin{cases} \dfrac{\sqrt{\bar{U}}}{\sqrt{U_A} + \sqrt{U_B}} e^{-|x|/\sqrt{U(x)}} & n = 1 \qquad (3.11a) \\ \left(\dfrac{n-1}{2}\sqrt{\dfrac{2}{n+1}}\dfrac{|x|}{\sqrt{U(x)}} + \left(\dfrac{\sqrt{\bar{U}}\sqrt{\frac{n+1}{2}}}{\sqrt{U_A} + \sqrt{U_B}} \right)^{-\frac{n-1}{n+1}} \right)^{-\frac{2n}{n-1}} & n \neq 1 \qquad (3.11b) \end{cases}$$

Once again, we can derive exact solutions for the velocity field, $u(x)$, by integrating the identity $\frac{du}{dx} = (U_B - U_A)w(x)$ on the intervals $x \in [-\infty, -\epsilon]$ and $x \in [+\epsilon, +\infty]$

$$u(x) = \begin{cases} U(x) + \left(\dfrac{\sqrt{U_A U_B}}{\bar{U}} - U(x) \right) e^{-|x|/\sqrt{U(x)}}, & n = 1 \\ U(x) - \operatorname{sgn}(x)\sqrt{U(x)}\dfrac{U_B - U_A}{\bar{U}}\sqrt{\dfrac{2}{n+1}}\left(\dfrac{n-1}{2}\sqrt{\dfrac{2}{n+1}}\dfrac{|x|}{\sqrt{U(x)}} + \left(\dfrac{\sqrt{\bar{U}}\sqrt{\frac{n+1}{2}}}{\sqrt{U_A} + \sqrt{U_B}} \right)^{-\frac{n-1}{n+1}} \right)^{\frac{2n}{n-1}}, & n \neq 1 \end{cases}$$

We depict these solutions and compare to numerical solutions in figure 4. They are similar to the driving stress step-change solutions, yet are asymmetric. Because the longitudinal coupling length is inversely proportional to friction coefficient, $\ell \sim C^{-\frac{n}{n+1}}$, the decrease in friction on the fast side of the boundary layer leads to an increase in the longitudinal coupling length ℓ. This asymmetry distinguishes the results of the friction step-change from the driving stress step-change problems. For a linear sliding law, $m = 1$, changes to the driving stress field lead to symmetric boundary layers, while changes to the friction field lead to asymmetric boundary layers, with a shorter longitudinal coupling length on the high friction side of the boundary layer than the low friction side. This distinctive asymmetry may be a conspicuous feature in the flow morphology of ice streams, distinguishing fast flow from fast basal slip versus high driving stress.

(iii) The impact of nonlinear rheology on stress coupling

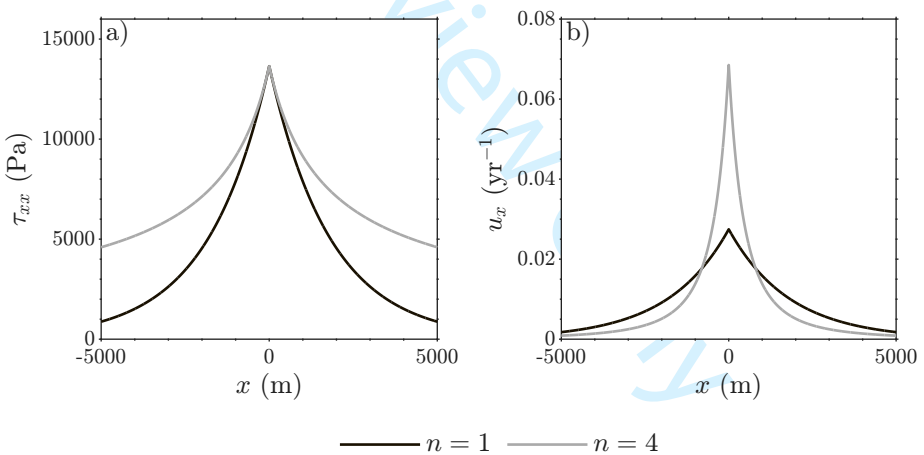

Figure 5. Exact solutions, in dimensional form, for linear Newtonian (black) and nonlinear ice (grey), in the case of an analogous boundary layer, where the maximum longitudinal stress and the velocity step change are equivalent between the linear and nonlinear problems. a) Deviatoric longitudinal stress. b) Longitudinal strain-rate.

We can determine the longitudinal deviatoric stress exactly, by putting our solutions back in dimensional form, calculating the strain-rate from $\frac{du}{dx} = (U_B - U_A)w$, and inserting it into rheology (2.1), for the expression

$$\tau_{xx} = A^{-1/n}|U_B - U_A|^{\frac{1-n}{n}}(U_B - U_A)w^{1/n}. \tag{3.13}$$

In this subsection, we briefly address 2 ambiguities that can arise from the results of our scaling analysis and exact solutions:

(1) There is a distinction between the strain-rate longitudinal-coupling length, ℓ, and the stress longitudinal-coupling length, which we will denote as L. ℓ is a characteristic length scale for

the strain-rate boundary layer. But because ice has a nonlinear rheology, there is a nonlinear relationship between the decay of the longitudinal strain-rate, $\frac{du}{dx}$, to the decay of the longitudinal deviatoric stress, τ_{xx}.

(2) Because of the nonlinear, shear-thinning rheology of ice, the strain-rate longitudinal coupling length, ℓ, is inversely proportional to the size of the velocity step-change, $\ell \sim |U_B - U_A|^{-\frac{n-1}{n+1}}$. Further, we observe that the nonlinear weighting functions decay faster than the linear weighting functions in figures (3- 4). This potentially gives the false impression that the nonlinear rheology acts to localize longitudinal stress when it actually causes the opposite by increasing the spatial extent of longitudinal deviatoric stress.

To address the impact of nonlinear rheology on the length scales of stress/strain-rate decay, we need a definition of the stress coupling length, L, that is consistent between the linear and nonlinear case. We adopt a definition from Rines et al. (2024; [12]), that L is the distance at which longitudinal stress has decayed to $1/e$ of its maximum value in the boundary layer.

For the linear case we find that the stress coupling lengthscale, $L_{n=1}$, is equivalent to the length scale $\ell_{n=1}$, since

$$A_{n=1}^{-1}\frac{U_B - U_A}{2\ell_{n=1}}e^{-1} = A_{n=1}^{-1}\frac{U_B - U_A}{2\ell_{n=1}}e^{-L_{n=1}/\ell_{n=1}}$$
$$L_{n=1} = \ell_{n=1} \tag{3.14}$$

meaning that our scaling ℓ is natural to the linear problem.

We define the stress coupling length for nonlinear ice, $L_{n\neq1}$, in the same way, as the distance at which longitudinal stress has decayed to $1/e$ of its maximum value. From this definition L and ℓ are not equal, with

$$L_{n\neq1} = \ell_{n\neq1} \cdot \frac{4}{n-1}\left(\frac{1}{2}\sqrt{\frac{n+1}{2}}\right)^{\frac{2}{n+1}}\left(e^{\frac{n-1}{2}} - 1\right), \tag{3.15}$$

related by a factor depending on n.

To compare values of $L_{n\neq1}$ between different shear thinning exponents n, we require a means to compare the viscosity parameter, A, between linear and nonlinear ice. For the linear case, the viscosity is constant throughout the domain, formulated as $\eta = \frac{1}{2A}$. For the non-linear case, viscosity is dependent on strain-rate, formulated as $\eta = \frac{1}{2}A^{-1/n}|\frac{du}{dx}|^{\frac{1-n}{n}}$. This highlights that A represents two fundamentally different quantities (with different dimensional units) between the Newtonian and non-Newtonian cases. For our purpose, since we are considering the decay of longitudinal stress forcings, we define values of $A_{n=1}$ which would lead to an equivalent maximum longitudinal stress for an equivalent velocity step-change between the Newtonian and non-Newtonian cases, $\tau_{xx}(0)_{n=1} = \tau_1(0)_{n\neq1}$, as illustrated by figure 5,

$$A_{n=1} = \frac{1}{4}A_{n\neq1}^{\frac{2}{n+1}}|U_B - U_A|^{\frac{2(n-1)}{n+1}}\left(\frac{2H}{C}\right)^{\frac{1-n}{n+1}}\left(\frac{1}{2}\sqrt{\frac{n+1}{2}}\right)^{-\frac{4}{n+1}}. \tag{3.16}$$

Next, we combine equations (3.15) and (3.16) to obtain

$$\frac{L_{n\neq1}}{L_{n=1}} = \frac{2}{n-1}\left(e^{\frac{n-1}{2}} - 1\right), \tag{3.17}$$

showing that the stress coupling length, $L_{n\neq1}$, for nonlinear, shear-thinning, viscous fluids is always longer than that of comparable Newtonian fluids, $L_{n=1}$ (figure 6).

The rheological exponent, n, is a fundamental quantity in determining the longitudinal coupling length. Larger values of n enhance the feedback between longitudinal stress and viscosity, which leads to higher longitudinal coupling lengths. n is often assumed to be constant in time in space, but ice flows as a result of several different mechanism, each with their own distinct value of n: dislocation creep ($n \approx 4$), grain boundary sliding ($n \approx 2$), and diffusion creep ($n = 1$) [36,39]. In ice sheet models, n is a parameterization that combines all of these processes

royalsocietypublishing.org/journal/rspa Proc R Soc A 0000000

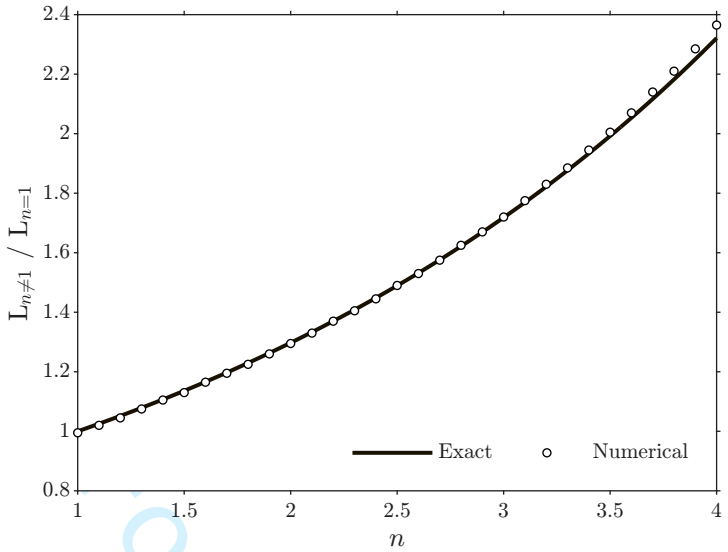

Figure 6. The ratio of the nonlinear stress LCL to the linear stress LCL, with respect to n. Solid line: analytic expression (3.17). Circle marker: numerical results.

in the aggregate. The spatial extent of longitudinal stress boundary layers may be a distinctive feature which can simplify inverse calculations of n from surface velocity observations [36].

For non-Newtonian ice, the strain-rate, $\frac{du}{dx}$, is localized and decays over a shorter length scale than its Newtonian counterpart. However, when comparing longitudinal stress from comparable baselines, the nonlinear stress coupling increases the LCL. This arises because $\tau_{xx} \sim \frac{du}{dx}^{1/n}$. Thus in the balance between localization and intensification of strain-rates, the intensification results in longer stress coupling lengths (but shorter strain-rate coupling lengths). Therefore, longitudinal stresses may be a significant portion of the stress balance over far greater distances than what may be apparent from surface velocity observations.

(b) Application to more complex forcings

Real glaciers and ice sheets contain spatially complex, multiscale, and co-occuring driving stress and friction fields, which complicate the idealized step-change boundary layer treatment. Here, we demonstrate that the step-change solutions are fundamental solutions to SSA, which help reconstruct the velocity field even under more realistic forcing.

While different constructions could manufacture solutions to SSA [40,41], step-changes correspond specifically to delta functions, $\delta(x)$, in gradients of momentum. In turn, our solutions have properties that closely resemble Green's functions. Indeed, for a linearly viscous, Newtonian fluid ($n = 1$), the exact solution (3.6) to the driving stress step-change problem (3.2) is exactly a Green's function, and can be used to write down exact solutions for more complex inhomogenous forcings, in the form of (2.5). Although Green's functions do not typically exist for nonlinear equations, we will demonstrate that our nonlinear solutions can approximately reconstruct the flow field, $u(x)$, under spatially complex driving stress and friction fields.

As an example, we consider a somewhat arbitrary complicated and continuous driving stress field, with constant basal friction, leading to the local velocity

$$U(x) = \frac{\tau_d(x)}{C} = \left(\bar{U} + \frac{U_B - U_A}{2}\tanh(x/500)\right)(1 + 0.1\sin(x/500)e^{-|x|/(10\ell)}). \tag{3.18}$$

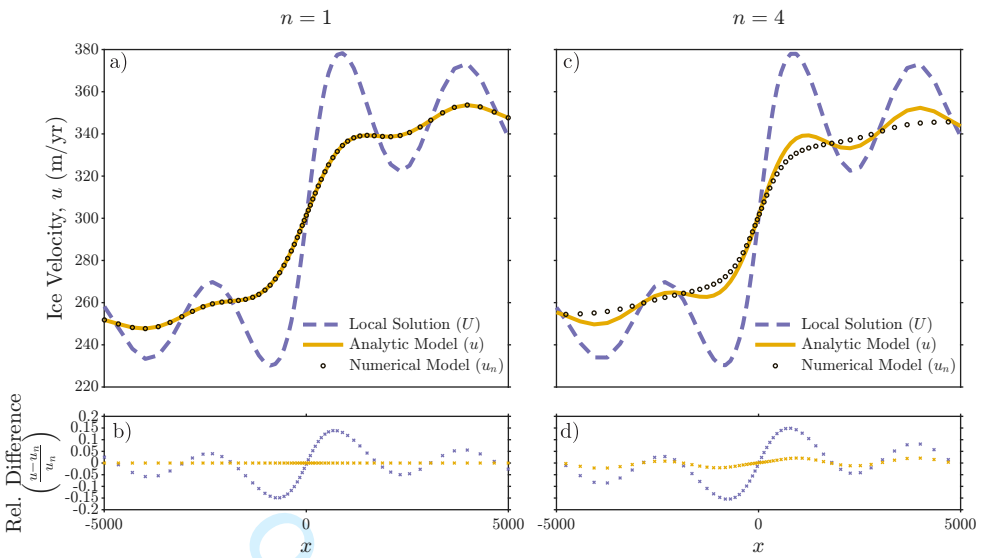

Figure 7. The local solution (3.18), numerical solution to SSA, and the analytic (Green's function) model subject to the local forcing. a) Solutions for linear ($n = 1$) Newtonian fluids. c) Solutions for nonlinear ($n = 4$), shear-thinning ice. b,d) Relative difference between the numerical solution vs. local solution (blue) and analytic model (orange).

We restate our ansatz (2.5), now as an approximate analytical model

$$u(x) \approx \int_{-\infty}^{+\infty} w(x-\xi)U(\xi)d\xi, \tag{3.19}$$

where w is given by (3.6). We numerically integrate (3.19) to solve for the velocity field, $u(x)$. Then, we compare the relative difference between our analytic model, u, and the numerical solution, u_n.

For linear-Newtonian ice ($n = 1$), Figure 7a demonstrates that w is indeed a Green's function, and our analytical model is an exact solution for arbitrary forcings, $U(x)$. For nonlinear ice ($n = 4$), Figure 7b demonstrates that, although not exact, our integral expression approximates the solution to the full SSA equations well, with a maximum $\sim 2\%$ relative difference between the integral and numerical models. Neglecting longitudinal stress and relying on the local model leads to a maximum $\sim 15\%$ relative difference. So, while the weighting function approach introduces some error, it does produce sensible results with considerably less computational expense than the fully numerical ice sheet model.

The surprising effectiveness of the weighted averaging approach suggests that, although the system is nonlinear, concepts like weighted averages, low-pass filters, and longitudinal coupling lengthscales still make sense as physical descriptions of nonlinear stress coupling, despite the fact that all of these concepts embed a kind of linear superposition in their underlying assumptions. For nonlinear viscous fluids, stress is not superimposed linearly, but this does not mean that stress is not superimposed at all. Frasca (2019; [42]) suggest that this type of solution to a delta function-forced, 2nd-order, nonlinear differential equations acts as the leading order term to an asymptotic expansion of the nonlinear Green's function.

Our semi-analytic model retains more information about the ice rheology than existing approaches, wherein a nonlinear rheology is linearized about a nonlinear background state [31], when large perturbations occur in the stress state. Our approach should always outperform assuming the local solution, as is done in (SIA) models, as long as a sensible value of ℓ is taken. While further refinement is possible, the nonlinear solutions are indeed fundamental solutions to the SSA boundary layer problem, which may have distinct advantages in interpreting surface velocity observations of fast flowing ice streams.

4. Discussion

In this study, we have developed a basic theory of stress coupling in glaciers and ice sheets, without assuming a linear rheology. We focus on fast flowing ice streams, well-described by the Shallow Shelf/Stream Approximation (SSA), and we find novel exact solutions to boundary layer problems involving a sudden change in either driving stress or friction. This analysis allows us to: (1) Determine the longitudinal coupling length precisely and (2) develop an approximate, semi-analytic model which can reconstruct the flow field for arbitrary driving stress fields.

(a) Model limitations and extensions

This work considers one-dimensional idealized ice streams that are infinite in extent and where ice thickness is held constant everywhere in the domain. Although real ice streams flow over variable bed topography and the ice surface evolves in time in response to surface mass balance processes and internal ice dynamics, these solutions can still be used to interpret regions where the variation in thickness is small compared to the the longitudinal coupling length, particularly in Siple Coast and other West Antarctic ice streams, which flow over flatter topography [43,44].

Our definition of the longitudinal coupling length and our exact solutions are both specific to the unconfined SSA model, with a linear sliding law, that we employ here. However, our approach is, in principle, applicable to any vertically integrated flowline glacier or ice sheet model. In future work, one could derive weighting functions for other ice sheet models, subject to different sliding laws and lateral confining stresses from the results of numerical ice sheet models.

Further, all of this analysis can be generalized from longitudinal to lateral profiles of the horizontal (x-direction) velocity, as a result of material frame invariance of the stress tensor (Appendix A.). This suggests that our longitudinal coupling length can be thought of more generally as a membrane (longitudinal and lateral shear) coupling length and applied to two-dimensional flow fields. Future work may be able to generalize this analysis towards two-dimensional exact solutions to SSA, which could fully unravel how membrane stresses superimpose in complex flow fields.

(b) Glaciological uses

The stress coupling length quantifies the spatial extent of perturbations to the stress field and thus diagnoses a kind of transmissivity of stress in ice [11–16,45,46]. Because the viscosity of ice is nonlinearly related to the stress state, the stress coupling length also nonlinearly coupled. Because we do not employ a linearly viscous model or linearize about a background nonlinear state, this work provides interpretations of the longitudinal coupling length that are applicable for large perturbations to the stress state.

The influence of nonlinear dynamics on longitudinal stress coupling provides a morphological interpretation of ice stream onset boundaries and shear margins. In the boundary layer between slower flow in the ice ridge and faster flow in the ice stream, there must be a change in friction and/or driving stress. The allows an interpretation of the magnitude and extent of longitudinal and membrane stress from surface velocity observations, but performing this calculation correctly requires accounting for explicitly nonlinear features.

One possible direct application is to 'cascading lake drainage' events in Greenland. During summer melt seasons, surface meltwater lakes initiate hydrofracture and drain water to the basal environment. This locally lubricates the bed and perturbs the stress state [47–56]. Extensional stresses caused by this local lubrication may cause a chain reaction, in which one drainage event triggers many more, as evidenced by observations of multiple successive lake hydrofracture events and some numerical modeling work [57,58]. Understanding the nonlinear dynamics that inform longitudinal coupling lengths assists us in determining the plausibility of this hypothesis. Further, our determination that the stress coupling length is always longer than the strain-rate

coupling length (when $n > 1$), tells us that stresses can be transmitted farther away from the hydrofracture than what may be immediately apparent from surface velocity observations.

An application of our simple boundary layer problems comes from using them to interpret the superposition of longitudinal and membrane stresses in complex flow fields. We demonstrate that the weighting functions, w, can act as a kind of inverse operator, fundamental solution, or Green's function for ice dynamics, relating complex and multi-scale forcings (driving stress and friction fields) to smooth and continuous outputs (velocity fields). For linearly viscous fluids, we have found a Green's function for SSA, and for nonlinear ice, we can employ the solution to construct approximate ice velocity fields in a manner which is always more effective than neglecting longitudinal stresses altogether and relying on the local solution. This method can be employed as a powerful and numerically cheap way to estimate the effect of longitudinal stress on ice flow fields, without resorting to direct numerical simulation. Future work could apply this method through top-down force balance considerations to derive longitudinal coupling lengths in real flow fields, as in other work [11].

These novel exact solutions should also be useful as numerical benchmarks. Direct comparison to an analytical solution can guide the development of optimal numerical solutions [59]. When the longitudinal coupling length is small, compared to the grid-resolution, some boundary layer processes are not well-resolved. These solutions can aid in the development of mesh refinement and subgrid parameterizations.

5. Conclusions

When ice flows across variable topography or friction, ice deformation is a function of nonlocal influences. This work considers nonlinear longitudinal stress coupling in fast, grounded ice stream flow. We derive exact solutions to the Shallow Shelf/Stream Approximation that clarify the longitudinal coupling length, which is the length scale over which perturbations to the stress state can effect the flow of distant ice. We take a shear thinning, power-law rheology for the ice, which allows us to focus on the effect of nonlinearity on stress coupling. Exact solutions show that rheological nonlinearities decrease the strain-rate coupling length, but increase the stress coupling length. This implies that boundary layers may transmit longitudinal stress farther away than what may be immediately apparent from surface velocity observations. Further, we show that we can reconstruct velocity fields for more complex continuous forcings. The use of the nonlinear solutions as Green's functions is surprisingly robust as a first-order approximation of longitudinal stress superposition, and can be used to interpret surface velocity observations in ice streams.

Appendix A. Lateral shear stress

The main text considers stress coupling in a 1D longitudinal profile, along the flowline of an ice stream without any confinement (no lateral stress). In this appendix section, we demonstrate that for a lateral profile subject to lateral shear stress, but no longitudinal stress, we can recover mathematically equivalent step-change problems, which determines the lateral coupling length.

In 2-dimensions, (x, y), SSA (or any vertically integrated model that uses the SSA horizontal stress balance) can be defined as an elliptic partial differential equation, for the vertically integrated velocity field, (u, v), in tensor form as [9,60]

$$\partial_j T_{ij}(D_{ij}) - C|u_i|^{m-1}u_i = -\tau_{d,i}, \tag{A.1}$$

where T_{ij} is a vertically integrated membrane stress tensor,

$$T_{ij} = 2\bar{\eta}(D_{ij})H\left(D_{ij} + (D_{11} + D_{22})\delta_{ij}\right), \tag{A.2}$$

$D_{ij} = \frac{1}{2}\left(\partial_i u_j + \partial_j u_i\right)$ is the vertically integrated strain-rate tensor, and $\bar{\eta} = \frac{1}{2A^{1/n}}[D_{11}^2 + D_{22}^2 + D_{11}D_{22} + D_{12}^2]^{\frac{1-n}{2n}}$ is the vertically integrated effective viscosity,

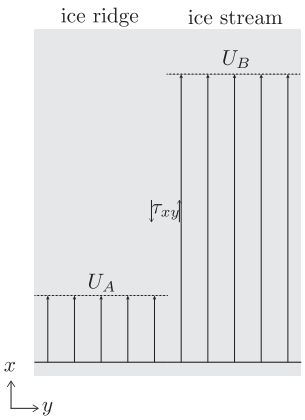

Figure 8. A schematic diagram for the lateral stress coupling problem, A.3.

We highlight that, if we consider a lateral cross section (instead of a longitudinal flow line) of an ice stream, with no variation in the x-direction, $\partial u/\partial x = 0$, and no lateral flow, $v = 0$, but instead variation in the y-direction of either the x-component of driving stress, $\tau_{dx}(y)$ or friction, $C(y)$, such as in an ice stream shear margin (figure 8), we recover a problem with the same structure to (2.2) for $u(y)$

$$\frac{d}{dy}\left(H(2A)^{-1/n}\left|\frac{du}{dy}\right|^{\frac{1-n}{n}}\frac{du}{dy}\right) - C(y)\,|u|^{m-1}\,u = -\tau_{dx}(y), \tag{A.3}$$

where lateral shear stresses take the place of longitudinal stresses. This is an expression of the material frame invariance of the vertically integrated stress tensor. So, while our analysis focuses on longitudinally variable ice flow, this work can be generalized to lateral variation, as in shear margins. While beyond the scope of this current paper, we hypothesize that our analysis could be operationalized towards a more general nonlinear analysis of membrane stresses in 2 dimensions.

Acknowledgements. We acknowledge support from the National Science Foundation (NSF) Graduate Research Fellowship Program (LEM; 2023313629), NSF–2012958 (CRM), Army Research Office (CRM; 78811EG), and the Grantham Foundation (CRM). KLPW was supported by a Dartmouth Society of Fellows fellowship and a Junior Research Fellowship (Trinity College Cambridge). We thank Ed Bueler for insightful conversations early in manuscript development.

References

1. Schoof C, Hindmarsh RC. 2010 Thin-film flows with wall slip: an asymptotic analysis of higher order glacier flow models. *Quarterly journal of mechanics and applied mathematics* **63**, 73–114.
2. Fowler A, Larson D. 1978 On the flow of polythermal glaciers-I. Model and preliminary analysis. *Proceedings of the Royal Society of London. A. Mathematical and Physical Sciences* **363**, 217–242.
3. Morland L, Johnson I. 1980 Steady motion of ice sheets. *Journal of Glaciology* **25**, 229–246.
4. Morland L, Shoemaker E. 1982 Ice shelf balances. *Cold Regions Science and Technology* **5**, 235–251.
5. Morland L. 1984 Thermomechanical balances of ice sheet flows. *Geophysical & Astrophysical Fluid Dynamics* **29**, 237–266.
6. Hutter K, Yakowitz S, Szidarovszky F. 1986 A numerical study of plane ice-sheet flow. *Journal of Glaciology* **32**, 139–160.
7. PIETRO ND, Cox R. 1979 The spreading of a very viscous liquid on a quiescent water surface. *The Quarterly Journal of Mechanics and Applied Mathematics* **32**, 355–381.
8. Weertman J. 1957 Deformation of floating ice shelves. *Journal of glaciology* **3**, 38–42.

9. MacAyeal DR. 1989 Large-scale ice flow over a viscous basal sediment: Theory and application to ice stream B, Antarctica. *Journal of Geophysical Research: Solid Earth* **94**, 4071–4087.
10. Kamb B, Echelmeyer KA. 1986 Stress-gradient coupling in glacier flow: I. Longitudinal averaging of the influence of ice thickness and surface slope. *Journal of Glaciology* **32**, 267–284.
11. Enderlin EM, Hamilton GS, O'Neel S, Bartholomaus TC, Morlighem M, Holt JW. 2016 An empirical approach for estimating stress-coupling lengths for marine-terminating glaciers. *Frontiers in Earth Science* **4**, 104.
12. Rines JH, Lai CY, Wang Y. 2024 Theoretical analysis of stress perturbations from a partially-lubricated viscous gravity current. *Journal of Fluid Mechanics (In Review)*.
13. Whillans IM, Johnsen SJ. 1983 Longitudinal variations in glacial flow: theory and test using data from the Byrd Station strain network, Antarctica. *Journal of Glaciology* **29**, 78–97.
14. Nye JF. 1969 The effect of longitudinal stress on the shear stress at the base of an ice sheet. *Journal of Glaciology* **8**, 207–213.
15. Budd W. 1970 The longitudinal stress and strain-rate gradients in ice masses. *Journal of Glaciology* **9**, 19–27.
16. Hutter K. 1981 The effect of longitudinal strain on the shear stress of an ice sheet: in defence of using stretched coordinates. *Journal of Glaciology* **27**, 39–56.
17. Echelmeyer KA, Kamb B. 1986 Stress-gradient coupling in glacier flow: II. Longitudinal averaging in the flow response to small perturbations in ice thickness and surface slope. *Journal of Glaciology* **32**, 285–298.
18. Kamb B. 1986 Stress-gradient coupling in glacier flow: III. Exact longitudinal equilibrium equation. *Journal of Glaciology* **32**, 335–341.
19. Kamb B, Echelmeyer KA. 1986 Stress-gradient coupling in glacier flow: IV. Effects of the "T" term. *Journal of Glaciology* **32**, 342–349.
20. O'Neel S, Pfeffer WT, Krimmel R, Meier M. 2005 Evolving force balance at Columbia Glacier, Alaska, during its rapid retreat. *Journal of Geophysical Research: Earth Surface* **110**.
21. Kavanaugh J, Cuffey K. 2009 Dynamics and mass balance of Taylor Glacier, Antarctica: 2. Force balance and longitudinal coupling. *Journal of Geophysical Research: Earth Surface* **114**.
22. Barcilon V, MacAyeal DR. 1993 Steady flow of a viscous ice stream across a no-slip/free-slip transition at the bed. *Journal of Glaciology* **39**, 167–185.
23. Bahr DB, Pfeffer WT, Meier MF. 1994 Theoretical limitations to englacial velocity calculations. *Journal of Glaciology* **40**, 509–518.
24. Jóhannesson T. 1992 *Landscape of temperate ice caps*. University of Washington.
25. Mantelli E, Haseloff M, Schoof C. 2019a Ice sheet flow with thermally activated sliding. Part 1: the role of advection. *Proceedings of the Royal Society A* **475**, 20190410.
26. Mantelli E, Bertagni MB, Ridolfi L. 2016 Stochastic ice stream dynamics. *Proceedings of the National Academy of Sciences* **113**, E4594–E4600.
27. Schoof C, Mantelli E. 2021 The role of sliding in ice stream formation. *Proceedings of the Royal Society A* **477**, 20200870.
28. Stubblefield AG, Wearing M, Meyer C. 2023a Linear analysis of ice-shelf topography response to basal melting and freezing. *Proceedings of the Royal Society A* **479**, 20230290.
29. Stubblefield AG, Meyer CR, Siegfried MR, Sauthoff W, Spiegelman M. 2023b Reconstructing subglacial lake activity with an altimetry-based inverse method. *Journal of Glaciology* pp. 1–15.
30. Hindmarsh RC. 1997 Normal modes of an ice sheet. *Journal of Fluid Mechanics* **335**, 393–413.
31. Gudmundsson GH. 2003 Transmission of basal variability to a glacier surface. *Journal of Geophysical Research: Solid Earth* **108**.
32. Hindmarsh R. 2004 A numerical comparison of approximations to the Stokes equations used in ice sheet and glacier modeling. *Journal of Geophysical Research: Earth Surface* **109**.
33. Crozier J, Karlstrom L, Yang K. 2018 Basal control of supraglacial meltwater catchments on the Greenland Ice Sheet. *The Cryosphere* **12**, 3383–3407.
34. Fowler AC. 2001 Modelling the flow of glaciers and ice sheets. In *Continuum mechanics and applications in geophysics and the environment* , pp. 201–221. Springer.
35. Goldsby D, Kohlstedt DL. 2001 Superplastic deformation of ice: Experimental observations. *Journal of Geophysical Research: Solid Earth* **106**, 11017–11030.
36. Millstein JD, Minchew BM, Pegler SS. 2022 Ice viscosity is more sensitive to stress than commonly assumed. *Communications Earth & Environment* **3**, 57.
37. Ham DA, Kelly PHJ, Mitchell L, Cotter CJ, Kirby RC, Sagiyama K, Bouziani N, Vorderwuelbecke S, Gregory TJ, Betteridge J, Shapero DR, Nixon-Hill RW, Ward CJ, Farrell

PE, Brubeck PD, Marsden I, Gibson TH, Homolya M, Sun T, McRae ATT, Luporini F, Gregory A, Lange M, Funke SW, Rathgeber F, Bercea GT, Markall GR. 2023 *Firedrake User Manual*. Imperial College London and University of Oxford and Baylor University and University of Washington first edition edition. (10.25561/104839)
38. Griffiths D, Walborn S. 1999 Dirac deltas and discontinuous functions. *American Journal of Physics* **67**, 446–447.
39. Schohn CM, Iverson NR, Zoet LK, Fowler JR, Morgan-Witts N. 2025 Linear-viscous flow of temperate ice. *Science* **387**, 182–185.
40. Böðvarsson G. 1955 On the flow of ice-sheets and glaciers. *Jökull* **5**, 1–8.
41. Bueler E. 2014 An exact solution for a steady, flowline marine ice sheet. *Journal of Glaciology* **60**, 1117–1125.
42. Frasca M, Khurshudyan AZ. 2019 A general representation for the Green's function of second-order nonlinear differential equations. *Computational and Mathematical Methods* **1**, e1038.
43. Shabtaie S, Bentley CR. 1987 West Antarctic ice streams draining into the Ross Ice Shelf: configuration and mass balance. *Journal of Geophysical Research: Solid Earth* **92**, 1311–1336.
44. Retzlaff R, Lord N, Bentley CR. 1993 Airborne-radar studies: Ice streams A, B and C, West Antarctica. *Journal of Glaciology* **39**, 495–506.
45. Budd W. 1971 Stress variations with ice flow over undulations. *Journal of Glaciology* **10**, 177–195.
46. McMeeking R, Johnson R. 1985 On the analysis of longitudinal stress in glaciers. *Journal of Glaciology* **31**, 293–302.
47. Zwally HJ, Abdalati W, Herring T, Larson K, Saba J, Steffen K. 2002 Surface melt-induced acceleration of Greenland ice-sheet flow. *Science* **297**, 218–222.
48. Joughin I, Das SB, King MA, Smith BE, Howat IM, Moon T. 2008 Seasonal speedup along the western flank of the Greenland Ice Sheet. *Science* **320**, 781–783.
49. van de Wal RS, Boot W, Van den Broeke M, Smeets C, Reijmer C, Donker J, Oerlemans J. 2008 Large and rapid melt-induced velocity changes in the ablation zone of the Greenland Ice Sheet. *science* **321**, 111–113.
50. Schoof C. 2010 Ice-sheet acceleration driven by melt supply variability. *Nature* **468**, 803–806.
51. Bartholomew I, Nienow P, Sole A, Mair D, Cowton T, King M, Palmer S. 2011 Seasonal variations in Greenland Ice Sheet motion: Inland extent and behaviour at higher elevations. *Earth and Planetary Science Letters* **307**, 271–278.
52. Hewitt I. 2013 Seasonal changes in ice sheet motion due to melt water lubrication. *Earth and Planetary Science Letters* **371**, 16–25.
53. Sole A, Nienow P, Bartholomew I, Mair D, Cowton T, Tedstone A, King MA. 2013 Winter motion mediates dynamic response of the Greenland Ice Sheet to warmer summers. *Geophysical Research Letters* **40**, 3940–3944.
54. Sergienko OV. 2013 Glaciological twins: basally controlled subglacial and supraglacial lakes. *Journal of Glaciology* **59**, 3–8.
55. Fitzpatrick AAW, Hubbard AL, Box J, Quincey DJ, Van As D, Mikkelsen A, Doyle SH, Dow C, Hasholt B, Jones GA. 2014 A decade (2002–2012) of supraglacial lake volume estimates across Russell Glacier, West Greenland. *The Cryosphere* **8**, 107–121.
56. Stevens LA, Behn MD, Das SB, Joughin I, Noël BP, van den Broeke MR, Herring T. 2016 Greenland Ice Sheet flow response to runoff variability. *Geophysical Research Letters* **43**, 11295–11303.
57. Christoffersen P, Bougamont M, Hubbard A, Doyle SH, Grigsby S, Pettersson R. 2018 Cascading lake drainage on the Greenland Ice Sheet triggered by tensile shock and fracture. *Nature Communications* **9**, 1064.
58. Stevens LA, Das SB, Behn MD, McGuire JJ, Lai CY, Joughin I, Larochelle S, Nettles M. 2024 Elastic stress coupling between supraglacial lakes. *Journal of Geophysical Research: Earth Surface* **129**, e2023JF007481.
59. Bueler E, Lingle CS, Kallen-Brown JA, Covey DN, Bowman LN. 2005 Exact solutions and verification of numerical models for isothermal ice sheets. *Journal of Glaciology* **51**, 291–306.
60. Bueler E, Brown J. 2009 Shallow shelf approximation as a "sliding law" in a thermomechanically coupled ice sheet model. *Journal of Geophysical Research: Earth Surface* **114**.

royalsocietypublishing.org/journal/rspa Proc R Soc A 0000000